Nonadiabatic dynamics for processes involving multiple avoided curve crossings: Double proton transfer and proton-coupled electron transfer reactions

Jian-Yun Fang and Sharon Hammes-Schiffer[a)]
Department of Chemistry and Biochemistry, University of Notre Dame, Notre Dame, Indiana 46556

(Received 24 June 1997; accepted 26 August 1997)

The extension of the surface hopping method ''molecular dynamics with quantum transitions'' (MDQT) to double proton transfer and proton-coupled electron transfer reactions is tested by comparison to fully quantum dynamical calculations for simple model systems. These model systems each include four potential energy surfaces and three or four avoided curve crossings. The agreement between the MDQT and fully quantum dynamical calculations provides validation for the application of MDQT to these biologically important processes. © *1997 American Institute of Physics.* [S0021-9606(97)50745-8]

I. INTRODUCTION

Quantum mechanical effects play an important role in many chemical processes in the condensed phase. Unfortunately, fully quantum mechanical simulations are computationally impractical for condensed phase systems. In many cases the significant quantum effects can be incorporated with mixed quantum/classical molecular dynamics methods, where one or a few degrees of freedom are treated quantum mechanically and the remainder of the system is treated classically. (See, for example, Refs. 1–20.) In these methods typically the instantaneous configuration of the classical subsystem determines the potential energy surface for the quantum subsystem, and in turn the quantum subsystem affects the evolution of the classical subsystem. In the adiabatic limit the system remains in a single adiabatic quantum state, and the classical particles evolve according to a potential obtained by averaging the potential energy over the occupied quantum state. For many chemical processes, however, the adiabatic approximation is invalid, so the development of methods that incorporate nonadiabatic effects is crucial. Surface hopping methods are mixed quantum/classical methods that incorporate nonadiabatic transitions between multiple potential surfaces.[19–36] In these methods typically an ensemble of trajectories is propagated, and each trajectory moves classically on a single adiabatic surface except for instantaneous transitions among the adiabatic states. The various surface hopping methods differ in the way in which the quantum transitions are incorporated and in the treatment of the phase coherence.

This paper is concerned with a particular surface hopping method called ''molecular dynamics with quantum transitions'' (MDQT).[19,32] In MDQT the quantum transitions are incorporated according to the ''fewest switches'' stochastic algorithm developed by Tully.[32] The standard MDQT method retains full coherence in the evolution of the quantum amplitudes. However, numerous methods for incorporating explicit decoherence effects have been utilized in conjunction with MDQT.[19,32] Surface hopping methods were initially developed for reactions evolving on multiple electronic surfaces.[32–34] MDQT has also been applied to proton transfer reactions in solution, where the transferring hydrogen atom is treated quantum mechanically and transitions are incorporated between the vibrational-like proton quantum states.[19,20] In addition to single proton transfer reactions, recently a multiconfigurational MDQT method (MC-MDQT) was developed for the simulation of multiple proton transfer reactions.[37,38] Moreover, recently MDQT was also applied to model proton-coupled electron transfer reactions, where transitions are incorporated between mixed proton/electron quantum states.[39,40]

Multiple proton transfer reactions and proton-coupled electron transfer reactions play an important role in a wide range of biological processes. For example, many enzyme reactions, including those involving serine proteases,[41,42] alcohol dehydrogenases,[43] and carbonic anhydrases,[44] require multiple proton transfer reactions. In addition, double proton transfer occurs in DNA base pairs such as the adenine-thymine base pair.[45] Moreover, the translocation of protons across biological membranes, which is important for photosynthesis[46–48] and respiration,[49–51] entails both multiple proton transfer reactions[52,53] and proton-coupled electron transfer. Another example of the biological importance of proton-coupled electron transfer is the conduction of electrons in cytochrome c, which is thought to involve interchain hops through hydrogen-bonded peptide residues of the protein.[54,55]

In this paper we test the extensions of MDQT to multiple proton transfer and proton-coupled electron transfer reactions by comparing MDQT and fully quantum dynamical calculations for simple model systems. The MDQT method has been compared to exact quantum dynamical calculations for simple one-dimensional two-state model systems representing processes evolving on multiple electronic surfaces.[32,34] Recently the MDQT method was compared to exact quantum dynamical calculations for a simple one-dimensional two-state model system representing a single proton transfer reaction.[56] The application of MDQT to multiple proton

[a)]Author to whom correspondence should be addressed.

transfer reactions and to proton-coupled electron transfer reactions differs from these previously studied model systems in that a larger number of potential energy surfaces and avoided curve crossings are involved. The treatment of phase coherence is critical for situations involving multiple avoided curve crossings due to the presence of quantum interference effects. Thus, these model systems provide a challenging test for mixed quantum/classical methods.

An outline of the paper is as follows. In Section II we discuss the MDQT and fully quantum wavepacket propagation methods. Section III presents a comparison of these two methods for two model systems representing double proton transfer and proton-coupled electron transfer reactions. Our conclusions are presented in Section IV.

II. METHODS

A. The MDQT Method

In this section we present a brief description of the MDQT method, which has been described in detail elsewhere.[19,32] For generality, we consider a system that is comprised of N quantum mechanical particles (with coordinates denoted by $\mathbf{r}$) and N_{cl} classical particles (with coordinates denoted by $\mathbf{R}$). The total Hamiltonian is

$$H = T_q + T_c + V(\mathbf{r},\mathbf{R}), \tag{1}$$

where T_q and T_c are the quantum and classical kinetic energies, respectively, and the total potential energy is $V(\mathbf{r},\mathbf{R})$. For each configuration $\mathbf{R}$ of the classical particles, the adiabatic quantum states $\Phi_n(\mathbf{r};\mathbf{R})$ and energies $E_n(\mathbf{R})$ can be calculated by solving the time-independent Schrödinger equation:

$$H_q \Phi_n(\mathbf{r};\mathbf{R}) = E_n(\mathbf{R}) \Phi_n(\mathbf{r};\mathbf{R}), \tag{2}$$

where

$$H_q = T_q + V(\mathbf{r},\mathbf{R}). \tag{3}$$

In MDQT the wave function $\Psi(\mathbf{r},\mathbf{R};t)$ that describes the quantum mechanical state at time t is expanded in terms of L orthonormal adiabatic states $\Phi_n(\mathbf{r};\mathbf{R})$:

$$\Psi(\mathbf{r},\mathbf{R};t) = \sum_{n=1}^{L} C_n(t) \Phi_n(\mathbf{r};\mathbf{R}), \tag{4}$$

where $C_n(t)$ are complex-valued expansion coefficients (i.e. quantum amplitudes). The quantum amplitudes $C_n(t)$ are propagated in time by integrating the time-dependent Schrödinger equation, which can be written in the following form:

$$i\hbar \dot{C}_k = \sum_{j=1}^{L} C_j (V_{kj} - i\hbar \dot{\mathbf{R}} \cdot \mathbf{d}_{kj}), \tag{5}$$

where

$$V_{kj}(\mathbf{R}) \equiv \langle \Phi_k(\mathbf{r};\mathbf{R}) | H_q | \Phi_j(\mathbf{r};\mathbf{R}) \rangle, \tag{6}$$

and the nonadiabatic coupling vector $\mathbf{d}_{kj}(\mathbf{R})$ is defined as:

$$\mathbf{d}_{kj}(\mathbf{R}) \equiv \langle \Phi_k(\mathbf{r};\mathbf{R}) | \nabla_{\mathbf{R}} \Phi_j(\mathbf{r};\mathbf{R}) \rangle. \tag{7}$$

The brackets denote integration over only the quantum mechanical coordinates $\mathbf{r}$.

The fundamental principle of MDQT is that an ensemble of trajectories is propagated on the adiabatic surfaces, and instantaneous transitions from one adiabatic surface to another are incorporated using a stochastic algorithm that ensures that the fraction in a given state j at a given time t is the quantum probability $|C_j(t)|^2$.[32] Thus, the system always remains in a particular adiabatic quantum state k, and the classical particles move according to classical equations of motion with a potential obtained by averaging the total potential over only the occupied adiabatic state. The quantum amplitudes $C_n(t)$ are propagated in time by integration of the time-dependent Schrödinger equation (Eq. 5) along the classical trajectory. At each classical time step, the ''fewest switches'' probabilistic algorithm[32] is used to determine if a switch to another adiabatic state should occur. If a switch does occur the classical velocities are scaled according to a force in the direction of the nonadiabatic coupling vector to maintain energy conservation. If the system attempts to switch to a state of higher energy and the required velocity reduction is greater than the component of the velocity to be adjusted, then the velocity component along the nonadiabatic coupling vector is reversed without switching states. The details of this method are described in Ref. 19.

The standard MDQT method retains full coherence in the evolution of the quantum amplitudes. As discussed in Ref. 32, this coherent evolution is essential for the reproduction of quantum interference effects. These interference effects are particularly important for processes involving multiple avoided curve crossings, as in the models described in this paper. On the other hand, quantum decoherence effects are expected to be important for condensed phase systems.[57,58] We explored several different methods for incorporating decoherence effects into the simulations presented in this paper. Our results indicate that for the one-dimensional model systems studied in this paper, quantum decoherence effects are negligible. Thus, we present results only for the standard MDQT method retaining full coherence.

B. Exact quantum dynamics in the adiabatic representation

Typically diabatic surfaces are utilized for fully quantum mechanical calculations on multiple potential surfaces.[59–61] For mixed quantum/classical simulations of condensed phase systems, however, the adiabatic representation is more convenient because the complete potential surfaces are not available, so the adiabatic basis functions $\phi_i(\mathbf{r};\mathbf{R})$ and eigenenergies are obtained locally ''on the fly'' during the simulation. Thus, in order to test the MDQT method the adiabatic representation is preferable.

Recently one of us developed a general method for fully quantum mechanical wavepacket propagation on multiple adiabatic potential surfaces.[56] This method was utilized to test MDQT for a simple model system representing a single proton transfer reaction in solution, which involved a single

avoided curve crossing. In this paper we utilize this method to test MDQT for model systems involving multiple avoided curve crossings. In this section we briefly outline the general methodology for fully quantum mechanical wavepacket propagation on multiple adiabatic potential surfaces.

Using the same notation as in the previous section, the total wavefunction $\Psi(\mathbf{r},\mathbf{R},t)$ can be expanded in terms of the L orthonormal real adiabatic basis functions $\phi_n(\mathbf{r};\mathbf{R})$ with time-dependent coefficients $\chi_k(\mathbf{R},t)$:

$$\Psi(\mathbf{r},\mathbf{R},t)=\sum_{k=1}^{L}\chi_k(\mathbf{R},t)\phi_k(\mathbf{r};\mathbf{R}). \tag{8}$$

Substituting this into the time-dependent Schrödinger equation leads to

$$i\hbar\frac{\partial\tilde{\chi}(\mathbf{R},t)}{\partial t}=\tilde{\mathscr{H}}\tilde{\chi}(\mathbf{R},t), \tag{9}$$

where $\tilde{\chi}(\mathbf{R},t)$ is an L-dimensional vector with elements $\chi_k(\mathbf{R},t)$ and $\tilde{\mathscr{H}}$ is an $L\times L$ matrix with elements

$$\mathscr{H}_{ij}(\mathbf{R})=K_{ij}(\mathbf{R})+V_{ij}(\mathbf{R})+D_{ij}(\mathbf{R})+G_{ij}(\mathbf{R}), \tag{10}$$

$$K_{ij}(\mathbf{R})=-\sum_{I=1}^{N}\frac{\hbar^2}{2M_I}\nabla^2_{\mathbf{R}_I}\delta_{ij}, \tag{11}$$

$$V_{ij}(\mathbf{R})=\langle\phi_i|H_q(\mathbf{r},\mathbf{R})|\phi_j\rangle, \tag{12}$$

$$D_{ij}(\mathbf{R})=-\sum_{I=1}^{N}\frac{\hbar^2}{M_I}\langle\phi_i|\nabla_{\mathbf{R}_I}\phi_j\rangle\nabla_{\mathbf{R}_I}, \tag{13}$$

and

$$G_{ij}(\mathbf{R})=-\sum_{I=1}^{N}\frac{\hbar^2}{2M_I}\langle\phi_i|\nabla^2_{\mathbf{R}_I}\phi_j\rangle. \tag{14}$$

Note that the brackets indicate integration over only the coordinates $\mathbf{r}$. For our calculations Eq. 9 is propagated with the Chebyshev method.[62]

In the adiabatic representation $V_{ij}=E_i\delta_{ij}$ and, in general, $D_{ij}\neq 0$ and $G_{ij}\neq 0$ so D_{ij} and G_{ij} must be evaluated. The matrix element required for the evaluation of D_{ij} is the standard nonadiabatic coupling vector that has been derived previously:

$$\left\langle\phi_i\left|\frac{\partial\phi_j}{\partial R_\mu}\right\rangle\right.=\frac{\langle\phi_i|\dfrac{\partial H_q}{\partial R_\mu}|\phi_j\rangle}{E_j-E_i} \tag{15}$$

for $i\neq j$ and

$$\left\langle\phi_i\left|\frac{\partial\phi_i}{\partial R_\mu}\right\rangle\right.=0. \tag{16}$$

Note that μ indicates the x, y, or z component of a particular slow coordinate $\mathbf{R}_I$. The derivation of analytical forms for the G_{ij} terms, which involve the calculation of $\langle\phi_i|(\partial^2/\partial R_\mu^2)|\phi_j\rangle$, is presented in Ref. 56. The off-diagonal terms $i\neq j$ can be expressed as

$$\begin{aligned}\left\langle\phi_i\left|\frac{\partial^2\phi_j}{\partial R_\mu^2}\right\rangle\right.=&\frac{\langle\phi_i|\dfrac{\partial^2 H_q}{\partial R_\mu^2}|\phi_j\rangle}{(E_j-E_i)}\\&+2\sum_{k\neq j}\frac{\langle\phi_i|\dfrac{\partial H_q}{\partial R_\mu}|\phi_k\rangle\langle\phi_k|\dfrac{\partial H_q}{\partial R_\mu}|\phi_j\rangle}{(E_j-E_k)(E_j-E_i)}\\&-2\frac{\langle\phi_j|\dfrac{\partial H_q}{\partial R_\mu}|\phi_j\rangle\langle\phi_i|\dfrac{\partial H_q}{\partial R_\mu}|\phi_j\rangle}{(E_j-E_i)^2},\end{aligned} \tag{17}$$

and the diagonal terms $i=j$ can be expressed as

$$\left\langle\phi_i\left|\frac{\partial^2\phi_i}{\partial R_\mu^2}\right\rangle\right.=-\sum_{k\neq i}\frac{\langle\phi_i|\dfrac{\partial H_q}{\partial R_\mu}|\phi_k\rangle^2}{(E_i-E_k)^2}. \tag{18}$$

Note that the calculation of the second-derivative G_{ij} terms does not involve the calculation of derivatives of the basis functions ϕ_i, but rather just the derivatives of the Hamiltonian H_q.

III. RESULTS AND DISCUSSION

In this section we compare MDQT to fully quantum dynamical calculations for two different systems involving multiple avoided curve crossings. The first system is a model for double proton transfer, and the second system is a model for proton-coupled electron transfer.

A. Double proton transfer

Our model for double proton transfer, as presented in Ref. 37, includes two proton degrees of freedom (r_1 and r_2) and one solvent degree of freedom (R), which represents a collective solvent mode. The Hamiltonian for this model is

$$\begin{aligned}H=&T_p+T_s+V_p(r_1)+V_p(r_2)+V_s(R)+V_{ps}(r_1,R)\\&+V_{pp}(r_1,r_2),\end{aligned} \tag{19}$$

where the subscripts p and s represent the proton and solvent degrees of freedom, respectively, and T and V are the kinetic and potential energy operators, respectively. (Note that T_p includes the kinetic energy of both protons.) The protons are of mass $m=1$ amu and move in double well potentials

$$V_p(r_i)=-0.5a_o r_i^2+0.25c_o r_i^4 \tag{20}$$

with $a_o=565$ Å^{-2} kcal/mol and $c_o=9975$ Å^{-4} kcal/mol, which corresponds to a barrier height of 8 kcal/mol, minima at ± 0.24 Å, and a frequency of 3650 cm^{-1} (typical of an OH stretching vibration). The solvent degree of freedom R is of mass $M=100$ amu and moves as a harmonic oscillator

$$V_s(R)=0.5M\omega R^2 \tag{21}$$

with $\omega=100$ cm^{-1}. The solvent degree of freedom is linearly coupled to one proton:

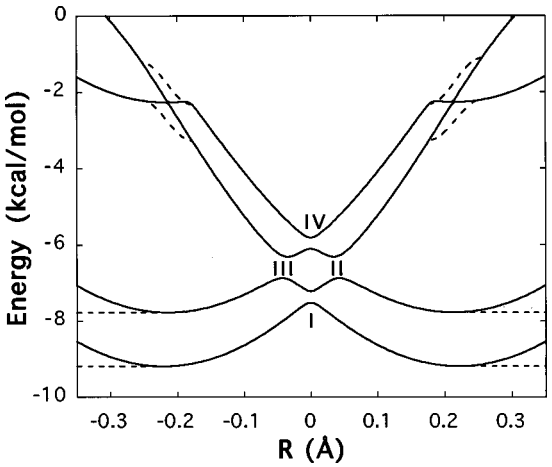

FIG. 1. The adiabatic potential energy curves as a function of the collective solvent coordinate R for the double proton transfer system. Only the four lowest energy adiabatic states are shown. In order to avoid numerical difficulties, the avoided crossing regions between the third and fourth states are smoothed out as shown by the dashed lines. In order to incorporate solvent-induced stabilization, the curves of the first two states are flattened for $|R|>0.21$ Å. The avoided crossing regions are labeled as I, II, III, and IV.

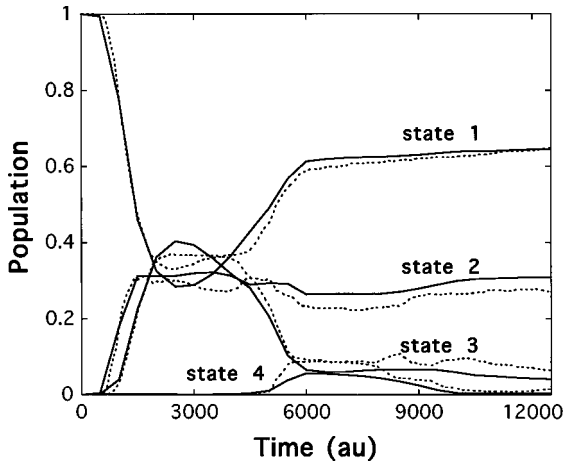

FIG. 2. The time evolution of the populations of the adiabatic states shown in Fig. 1 for fully quantum (solid lines) and MDQT (dashed lines) calculations with initial average momentum $P_o=40$ a.u. The other initial conditions and the stopping conditions are described in the text.

$$V_{ps}(r_1,R)=k_{ps}r_1R, \tag{22}$$

where $k_{ps}=83.33$ Å^{-2} kcal/mol. The two protons are also linearly coupled to each other:

$$V_{pp}(r_1,r_2)=k_{pp}r_1r_2 \tag{23}$$

with $k_{pp}=14.35$ Å^{-2} kcal/mol. (Reference 63 suggests that linear coupling between protons is physically reasonable for modeling systems such as multiple proton transfer reactions in chains of water molecules.)

Figure 1 presents the potential energy curves for the first four adiabatic states. These curves were obtained by solving the time-independent Schrödinger equation (Eq. 2). We performed both MDQT and fully quantum dynamical calculations for this system. For the MDQT calculations the protons were treated quantum mechanically, and the solvent mode was treated classically. Our interest is focused on the region around $R=0.0$ Å, where there are four avoided curve crossings. In order to avoid numerical difficulties, the avoided curve crossings between the third and fourth states at $|R|\sim 0.22$ Å were smoothed out. Moreover, in a condensed phase system solvent-induced stabilization would cause the system to remain in the stable state rather than to immediately react again. We incorporated this solvent-induced stabilization into our calculations by flattening the potential curves of the first and second states at $|R|>0.21$ Å. For the fully quantum dynamical calculations, absorbing boundaries were placed on all states at $R=\pm 0.20$ Å.[64] In the MDQT calculations, the trajectories were stopped once they reached the region with $|R|>0.20$ Å.

The initial wavepacket for the fully quantum wavepacket propagation was on the ground state and of the form

$$\chi_1(R)=\left(\frac{2\alpha}{\pi}\right)^{\frac{1}{4}} e^{-\alpha(R-R_o)^2+iP_o(R-R_o)/\hbar}, \tag{24}$$

where R_o, P_o, and α are parameters corresponding to the center, momentum, and width, respectively, of this wavepacket. For our simulations $\alpha=150$ a.u.$^{-2}$, $R_o=-0.25$ a.u., and the momentum $P_o=30$ a.u. or 40 a.u. The corresponding initial conditions for the MDQT simulations were chosen according to the Wigner representation of this initial wavepacket. 1020 MDQT trajectories were propagated for $P_o=30$ a.u., and 992 MDQT trajectories were propagated for $P_o=40$ a.u.

Figures 2 and 3 depict the time evolution of the populations on the first four states for both the MDQT and the fully quantum dynamical calculations for two different initial av-

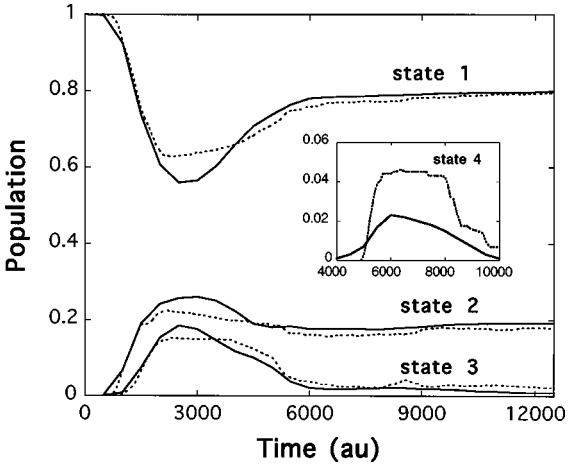

FIG. 3. The time evolution of the populations of the adiabatic states shown in Fig. 1 for fully quantum (solid lines) and MDQT (dashed lines) calculations with initial average momentum $P_o=30$ a.u. The other initial conditions and the stopping conditions are described in the text.

erage momenta ($P_o=40$ a.u. and $P_o=30$ a.u.). Since the wavepacket is initially on the ground state, the populations on the other states are zero at $t=0$. When the system enters the nonadiabatic coupling region the second, third, and fourth states become populated. At longer times most of the population on the third and fourth states drops back down to the ground state. One interesting feature of this system is that the population on the second state remains almost constant after a short initialization period. Thus, the second state mainly serves as a mediator for the population exchange between the ground and the third and fourth states. Note that the greatest discrepancies occur in the avoided crossing region. In general, when trajectories are in the strong nonadiabatic coupling region MDQT does not accurately describe the dynamics because in MDQT the trajectories are always moving according to forces due to a single adiabatic state. However, Figures 2 and 3 illustrate that MDQT accurately calculates the final branching probabilities. Overall, the agreement between MDQT and fully quantum calculations is very good with a maximum difference of 5%–7%, while the statistical error for 1000 trajectories is ~3%.

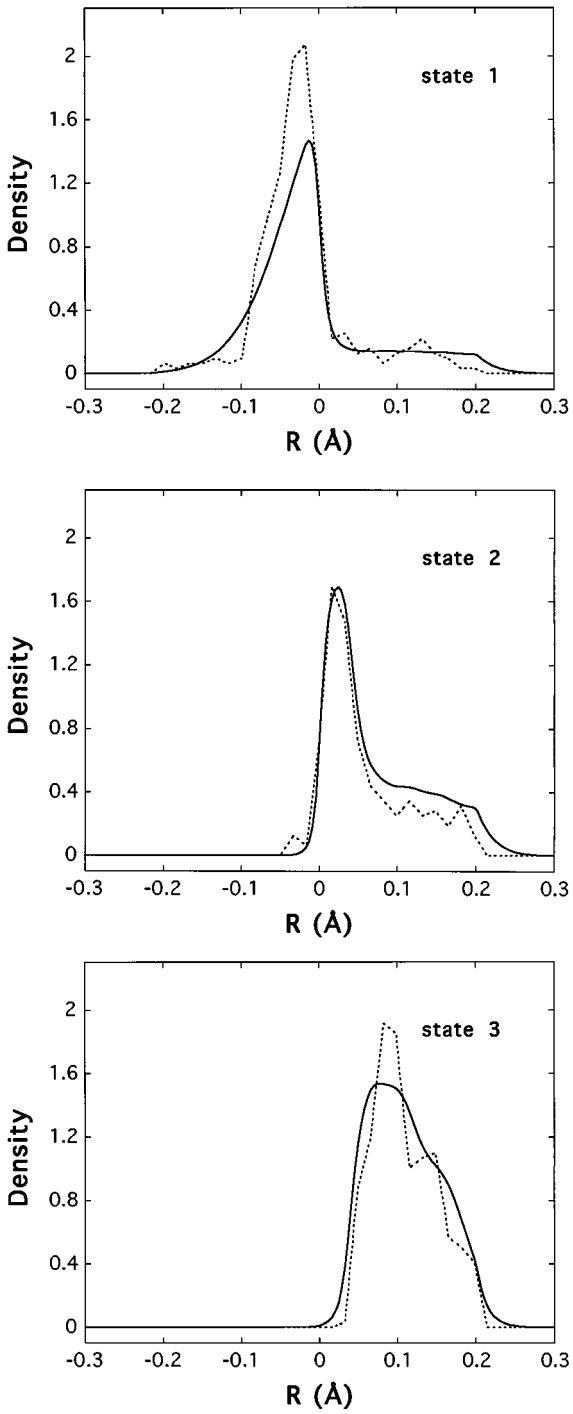

FIG. 4. The density distributions at time $t=3000$ a.u. for states 1, 2, and 3 shown in Fig. 1 for fully quantum (solid lines) and MDQT (dashed lines) calculations with initial average momentum $P_o=40$ a.u.

In Fig. 4, we compare the density distributions ($|\chi_k(R,t)|^2$) at a specified time for the MDQT and the fully quantum dynamical calculations. The MDQT density distribution is obtained by summing over the ensemble of trajectories for each point along the discrete coordinate grid at the specified time. The results shown are for the wavepacket with the initial average momentum $P_o=40$ a.u. at time t=3000 a.u. for the first three states. (The fourth state is not significantly populated at this time.) Similar results were obtained for the initial momentum $P_o=30$ a.u. and at different times. Since no renormalization is included, the discrepancies in the populations depicted in Fig. 2 are also evident in Fig. 4. Nevertheless, the agreement of the line shapes is qualitatively reasonable.

B. Proton-coupled electron transfer

Our one-dimensional model for proton-coupled electron transfer, as presented in Ref. 39, includes one proton coordinate (r_p), one electron coordinate (r_e), and one solvent degree of freedom (R), which represents a collective solvent mode. The electron donor D and acceptor A are fixed at a distance $d_{DA}=8.0$ a.u., and the proton donor and acceptor are also implicitly fixed on the D-A axis. The electron and proton are constrained to move in one dimension along this axis. The Hamiltonian for this model is

$$H=T_{pe}+T_s+V_s(R)+V_p(r_p)+V_e(r_e)+V_{pe}(r_p,r_e)+V_{pes}(r_p,r_e,R), \tag{25}$$

where the subscripts p, e, and s represent the proton, electron, and solvent degrees of freedom, respectively, and T and V are the kinetic and potential energy operators, respectively. The solvent potential is a simple harmonic oscillator potential

$$V_s(R)=\tfrac{1}{2}m_s\omega_s^2(R-R_o)^2, \tag{26}$$

where the mass $m_s=12.0$ amu, $\omega_s=0.0004$ a.u. and $R_o=-0.3$ a.u.. The proton potential V_p is a double well function represented by the quartic polynomial

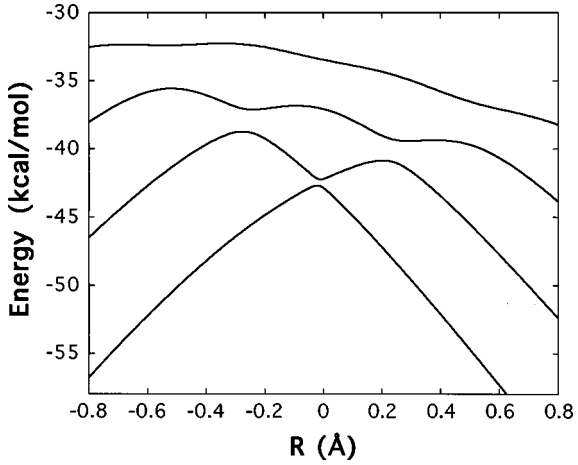

FIG. 5. The adiabatic potential energy curves as a function of the collective solvent coordinate R for the proton-coupled electron transfer system. Only the four lowest energy adiabatic states are shown.

$$V_p(r_p)=\frac{12\Delta E}{(a_2-a_1)^3(2a_3-a_1-a_2)}\left\{\frac{r_p^4}{4}-(a_1+a_2+a_3)\frac{r_p^3}{3}+(a_1a_2+a_1a_3+a_2a_3)\frac{r_p^2}{2}-(a_1a_2a_3)r_p+a_2^2[a_2^2-2a_2(a_1+a_3)+6a_1a_3]/12\right\}, \tag{27}$$

where $a_1=3.5$ a.u., $a_2=4.0$ a.u., $a_3=4.5$ a.u., and $\Delta E=0.012$ a.u.. The electron potential V_e is the sum of the Coulombic interactions between the electron and its donor and acceptor:

$$V_e(r_e)=-\frac{C_eC_D\ \mathrm{erf}(r_{eD})}{r_{eD}}-\frac{C_eC_A\ \mathrm{erf}(r_{eA})}{r_{eA}}, \tag{28}$$

where $C_e=0.15$ a.u., $C_D=0.55$ a.u., and $C_A=0.55$ a.u. are the absolute values of the effective charges on the electron, the donor, and the acceptor and r_{eD} and r_{eA} are the distances between the electron and the donor and acceptor. For numerical stability, we also included a repulsive term to prevent the electron from traveling too far beyond the donor and acceptor. This term is of the form $\exp[-5.0(r_e+5.0)]+\exp[-5.0(d_{DA}-r_e+5.0)]$, where all distances are in atomic units. The electron-proton interaction V_{pe} is also treated as a Coulombic interaction:

$$V_{pe}(r_p,r_e)=-\frac{C_pC_e\ \mathrm{erf}(r_{pe})}{r_{pe}}, \tag{29}$$

where again $C_p=0.15$ a.u. and $C_e=0.15$ a.u. are the absolute values of the effective charges of the proton and the electron and r_{pe} is the distance between the electron and the proton. Finally, the solvent mode is linearly coupled to the proton and the electron:

$$V_{pes}(r_p,r_e,R)=-C_{sp}(R-R_p^o)(r_p-r_p^o)-C_{se}(R-R_e^o)(r_e-r_e^o), \tag{30}$$

where $C_{sp}=0.03$ a.u., $C_{se}=0.004$ a.u., $R_p^o=0.0$ a.u., $R_e^o=-0.6$ a.u., $r_p^o=4.0$ a.u., and $r_e^o=4.0$ a.u. Other studies of proton-coupled electron transfer reactions have also described the interaction between the solvent and the proton or electron with a linear coupling term.[65] Although linear coupling is a substantial simplification of this interaction, it provides a physically reasonable description of the interaction of the fluctuating field of the solvent (represented by R in Eq. 30) with the electronic (or proton) charge distribution of the solute.

Figure 5 depicts the adiabatic potential curves for the first four quantum states. We performed both MDQT and fully quantum dynamical calculations for this system. For the MDQT calculations the proton and electron coordinates were treated quantum mechanically, while the solvent coordinate was treated classically. The initial wavepacket for the fully quantum calculations was a Gaussian function of the form in Eq. 24 on the ground state with $\alpha=25$ a.u., $R_0=-0.95$ a.u., and $P_0=23.5$ a.u. The MDQT calculations included 837 trajectories sampled from the Wigner distribution associated with this initial wavepacket. Figure 6 compares the populations on the first three states for the MDQT and fully quantum dynamical calculations as functions of time. The fourth state is not significantly populated throughout the dynamics. As for the previous model, the discrepancies between the MDQT and the fully quantum calculations are not substantially larger in magnitude than the statistical error for 837 trajectories.

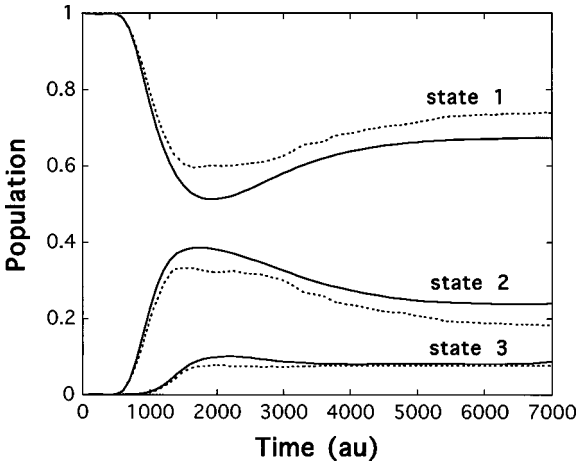

FIG. 6. The time evolution of the populations of the three lowest adiabatic states shown in Fig. 5 for fully quantum (solid lines) and MDQT (dashed lines) calculations with initial conditions as described in the text. (The fourth state is not significantly populated.)

IV. CONCLUSIONS

We have applied both MDQT and fully quantum dynamical methods to model systems for double proton transfer and proton-coupled electron transfer reactions. These model systems each involve four coupled adiabatic potential energy surfaces and three or four avoided curve crossings. The agreement between the MDQT and the fully quantum dynamical calculations provides validation for the application

of MDQT to these biologically important processes. These model systems, however, include only a single collective solvent mode and thus do not accurately incorporate dissipative effects that are present in condensed phase systems. The comparison of MDQT to exact quantum calculations for proton transfer in a dissipative system[66] will provide further validation of the application of MDQT to charge transfer reactions in the condensed phase.

ACKNOWLEDGMENTS

We acknowledge financial support from the NSF CAREER program Grant No. CHE-9623813, the Petroleum Research Fund (administered by the ACS) Grant No. 30432-G6, and the Clare Boothe Luce Foundation.

[1] M. Morillo and R. I. Cukier, J. Chem. Phys. **92**, 4833 (1990).
[2] A. Suárez and R. Silbey, J. Chem. Phys. **94**, 4809 (1991).
[3] A. Warshel and Z. T. Chu, J. Chem. Phys. **93**, 4003 (1990).
[4] J. Aqvist and A. Warshel, Chem. Rev. **93**, 2523 (1993).
[5] D. G. Truhlar, Y.-P. Liu, G. K. Schenter, and B. C. Garrett, J. Phys. Chem. **98**, 8396 (1994).
[6] D. Borgis, G. Tarjus, and H. Azzouz, J. Chem. Phys. **97**, 1390 (1992).
[7] D. Laria, G. Ciccotti, M. Ferrario, and R. Kapral, J. Chem. Phys. **97**, 378 (1992).
[8] D. Borgis and J. T. Hynes, Chem. Phys. **170**, 315 (1993).
[9] J. Mavri, H. J. C. Berendsen, and W. F. van Gunsteren, J. Phys. Chem. **97**, 13 469 (1993).
[10] A. Staib, D. Borgis, and J. T. Hynes, J. Chem. Phys. **102**, 2487 (1995).
[11] K. Ando and J. T. Hynes, J. Mol. Liquid **64**, 25 (1995).
[12] P. Bala, P. Grochowski, B. Lesyng, and J. A. McCammon, J. Phys. Chem. **100**, 2535 (1996).
[13] D. Li and G. A. Voth, J. Phys. Chem. **95**, 10 425 (1991).
[14] J.-K. Hwang and A. Warshel, J. Phys. Chem. **97**, 10 053 (1993).
[15] J.-K. Hwang, Z. T. Chu, A. Yadav, and A. Warshel, J. Phys. Chem. **95**, 8445 (1991).
[16] J. Lobaugh and G. A. Voth, J. Chem. Phys. **100**, 3039 (1994).
[17] H. Azzouz and D. Borgis, J. Chem. Phys. **98**, 7361 (1993).
[18] R. Pomés and B. Roux, Chem. Phys. Lett. **234**, 416 (1995).
[19] S. Hammes-Schiffer and J. C. Tully, J. Chem. Phys. **101**, 4657 (1994).
[20] S. Hammes-Schiffer and J. C. Tully, J. Phys. Chem. **99**, 5793 (1995).
[21] J. C. Tully and R. K. Preston, J. Chem. Phys. **55**, 562 (1971).
[22] W. H. Miller and T. F. George, J. Chem. Phys. **56**, 5637 (1972).
[23] J. R. Stine and J. T. Muckerman, J. Chem. Phys. **65**, 3975 (1976).
[24] N. C. Blais, D. G. Truhlar, and C. A. Mead, J. Chem. Phys. **89**, 6204 (1988).
[25] L. J. Dunne, J. N. Murrell, and J. G. Stamper, Chem. Phys. Lett. **112**, 497 (1984).
[26] M. F. Herman, J. Chem. Phys. **81**, 754 (1984).
[27] M. F. Herman and E. Kluk, in *Dynamical Processes in Condensed Matter*, edited by M. Evans (Wiley, New York, 1985), p. 577.
[28] J. C. Arce and M. F. Herman, J. Chem. Phys. **101**, 7520 (1994).
[29] G. Parlant and E. A. Gislason, J. Chem. Phys. **91**, 4416 (1989).
[30] G. Parlant and M. H. Alexander, J. Chem. Phys. **92**, 2287 (1990).
[31] P. J. Kuntz and J. J. Hogreve, J. Chem. Phys. **95**, 156 (1991).
[32] J. C. Tully, J. Chem. Phys. **93**, 1061 (1990).
[33] F. Webster, P. J. Rossky, and R. A. Friesner, Comput. Phys. Commun. **63**, 494 (1991); F. J. Webster, J. Schnitker, M. S. Friedrichs, R. A. Friesner, and P. J. Rossky, Phys. Rev. Lett. **66**, 3172 (1991).
[34] D. F. Coker, in *Computer Simulation in Chemical Physics*, edited by M. P. Allen and D. J. Tildesley (Kluwer Academic, Dordrecht, 1993), p. 315.
[35] B. Space and D. F. Coker, J. Chem. Phys. **94**, 1976 (1991).
[36] D. F. Coker and L. Xiao, J. Chem. Phys. **102**, 496 (1995).
[37] S. Hammes-Schiffer, J. Chem. Phys. **105**, 2236 (1996).
[38] K. Drukker and S. Hammes-Schiffer, J. Chem. Phys. **107**, 363 (1997).
[39] J.-Y. Fang and S. Hammes-Schiffer, J. Chem. Phys. **106**, 8442 (1997).
[40] J.-Y. Fang and S. Hammes-Schiffer, J. Chem. Phys. **107**, 5727 (1997).
[41] D. M. Blow, Acc. Chem. Res. **9**, 145 (1976).
[42] G. Zundel, J. Mol. Struct. **177**, 43 (1988).
[43] S. Ramaswamy, H. Eklund, and B. V. Plapp, Biochemistry **33**, 5130 (1994).
[44] X. Ren, C. Tu, P. J. Laipis, and D. N. Silverman, Biochemistry **34**, 8492 (1995).
[45] J. Floriń, V. Hrouda, and P. Hobza, J. Am. Chem. Soc. **116**, 1457 (1994).
[46] G. T. Babcock, B. A. Barry, R. J. Debus, C. W. Hoganson, M. Atamian, L. McIntosh, I. Sithole, and C. F. Yocum, Biochemistry **28**, 9557 (1989).
[47] M. Y. Okamuraand G. Feher, Annu. Rev. Biochem. **61**, 861 (1992).
[48] C. Kirmaier and D. Holten, in *The Photosynthetic Bacterial Reaction Center—Structure and Dynamics*, edited by J. Breton and A. Vermeglio (Plenum, New York, 1988).
[49] M. Wikstrom, Nature (London) **338**, 776 (1989).
[50] G. T. Babcock and M. Wikstrom, Nature (London) **356**, 301 (1992).
[51] B. G. Malmstrom, Acc. Chem. Res. **26**, 332 (1993).
[52] L. Baciou and H. Michel, Biochemistry **34**, 7967 (1996).
[53] R. A. Mathies, S. W. Lin, J. B. Ames, and W. T. Pollard, Annu. Rev. Biophys. Biophys. Chem. **20**, 491 (1991).
[54] M. J. Therien, M. Selman, H. B. Gray, I.-J. Chang, and J. R. Winkler, J. Am. Chem. Soc. **112**, 2420 (1990).
[55] J. N. Onuchic and D. N. Beratan, J. Chem. Phys. **92**, 722 (1990).
[56] J. Morelli and S. Hammes-Schiffer, Chem. Phys. Lett. **269**, 161 (1997).
[57] E. R. Bittner and P. J. Rossky, J. Chem. Phys. **103**, 8130 (1995).
[58] B. J. Schwartz, E. R. Bittner, O. V. Prezhdo, and P. J. Rossky, J. Chem. Phys. **104**, 5942 (1996).
[59] Z. Kotler, A. Nitzan, and R. Kosloff, Chem. Phys. Lett. **153**, 483 (1988).
[60] J. Campos-Martinez, J. R. Waldeck, and R. D. Coalson, J. Chem. Phys. **96**, 3613 (1992).
[61] J.-Y. Fang and H. Guo, J. Chem. Phys. **101**, 5831 (1994).
[62] H. Tal-Ezer and R. Kosloff, J. Chem. Phys. **81**, 3967 (1984).
[63] X. Duan and S. Scheiner, J. Mol. Struct. **270**, 173 (1992).
[64] R. Kosloff and D. Kosloff, J. Comput. Phys. **63**, 363 (1986).
[65] R. I. Cukier, J. Phys. Chem. **99**, 16 101 (1995).
[66] M. Topaler and N. Makri, J. Chem. Phys. **101**, 7500 (1994).